IEEE Access
Multidisciplinary | Rapid Review | Open Access Journal

Received 13 January 2025, accepted 23 February 2025, date of publication 27 February 2025, date of current version 7 March 2025.

Digital Object Identifier 10.1109/ACCESS.2025.3546520

RESEARCH ARTICLE

A Novel CNN-Based Framework for Detection and Classification of Power Quality Disturbances: Exploring Multi-Class Versus Multi-Label Classification

ALEKSANDRA ZLATKOVA, (Member, IEEE), AND DIMITAR TASKOVSKI, (Senior Member, IEEE)

Faculty of Electrical Engineering and Information Technologies, Ss. Cyril and Methodius University in Skopje, 1000 Skopje, North Macedonia

Corresponding author: Aleksandra Zlatkova (aleksandraz@feit.ukim.edu.mk)

This work was supported by European Union under Grant 101136775.

ABSTRACT The detection and classification of power quality (PQ) disturbances remains a significant challenge because of the rapid integration of renewable energy sources (RES), widespread use of power electronics, and increasing prevalence of sensitive microcontrollers. These evolving PQ issues necessitate the development of accurate and reliable methods for identifying and classifying PQ disturbances. In this paper, we propose a novel model based on a deep convolutional neural network (DCNN) for the feature extraction and classification of PQ disturbances. The architecture of the model was inspired by the visual geometry group (VGG), which is known for its effectiveness in image processing. The extracted features are highly suitable for both multi−class (MC) and multi−label (ML) classification tasks, effectively addressing the complexity of PQ disturbance signals. The ML approach proved its excellence in the classification of complex PQ disturbances. The performance of the model was rigorously evaluated using various metrics across different scenarios, which demonstrated exceptional accuracy and robustness. The model was trained, validated, and tested using synthetically generated data under different signal−to−noise ratio (SNR) scenarios ensuring its effectiveness in practical applications.

INDEX TERMS Convolutional neural network, deep learning, multi-class classification, multi-label classification, power quality.

I. INTRODUCTION

The increasing number of renewable energy sources (RES) in the electric grid and other factors such as the incorporation of power electronics and nonlinear loads, have led to faster development of the electrical grid, however such advances pose major power quality (PQ) challenges that undermine the stability and reliability of the power grid. Electric PQ disturbances are distortions of the voltage or current caused by any changes in amplitude, frequency or waveform to the limits of PQ international standards [1], [2]. In particular, the integration of RES contributes to various PQ disturbances such as sags, swells, interruptions, flicker, and harmonic distortion [3], [4]. However, these PQ issues can arise from multiple sources [5], underscoring the need for a real−time monitoring system capable of effectively detecting, classifying, and addressing these disturbances. Currently, grid stakeholders monitor PQ in real time, without automated data analysis [6]. This approach is time consuming, and large volumes of data are stored without efficient processing. Therefore, the proposed solution should be characterized by real−time identification with high performance in noisy environments. The detection and classification of PQ disturbances are generally performed in three steps: signal preprocessing, feature extraction, and classification. Signal preprocessing typically encompasses normalization, denoising, and

The associate editor coordinating the review of this manuscript and approving it for publication was Ahmed A. Zaki Diab.

phase correction to prepare a signal for accurate feature extraction and classification. Noise and phase shifts significantly affect the accuracy of the proposed model [7], [8]. Commonly employed signal processing (SP) methods include the wavelet transform (WT), Hilbert-Huang transform (HHT), and s-transform (ST) [7], [8], [9], [10]. Although WT offers excellent time−frequency resolution and is widely utilized, its performance deteriorates in noisy environments. Although ST is efficient for feature extraction, its high computational complexity makes it unsuitable for real−time application. Classification is typically achieved using machine learning as a support vector machine (SVM), decision tree (DT), random forest (RF), artificial neural networks (ANN), etc. [11], [12], [13], [14], [15]. However, despite their high efficiency, the performance of these classifiers primarily depends on the quality of the extracted features. In recent years, deep learning (DL) has gained popularity in PQ analysis owing to its success in computer vision tasks. Researchers are increasingly using SP techniques to convert one dimensional (1D) signals into images, which are then fed into DL models for classification [16], [17], [18]. Convolutional neural networks (CNN), long short−term memory (LSTM) and gated recurrent unit (GRU) have become particularly prominent in the detection and classification of PQ disturbances, to achieve a high accuracy and reliability. In [19], a model based on a 1D CNN was proposed for the classification of 16 single and complex PQ disturbances. In [20], an ensemble CNN (ECNN) was introduced to classify PQ disturbances originating from and negatively affecting electric vehicle charging. In [18] ST was employed to transform a 1D signal into an image, which was then used as an input for the residual network (ResNet) and modified ResNet architectures for feature extraction. In the modified ResNet, the channels are split into groups, and separate convolutional filters are applied to each group to decrease computational complexity. A novel algorithm inspired by inception ResNet was proposed in [21] and, demonstrated improved performance and generalization. A five−layer modified inception−ResNet is proposed for the classification of eight PQ disturbances. This architecture accepts a 1D signal as input. The proposed model achieves an accuracy of around 98%. Furthermore, the model is tested for the classification of composite PQ disturbances. However, it is not well explained how the proposed architecture classifies composite disturbances when the model has eight outputs and uses a softmax activation function in the final fully connected layer (FC). In [22], an auto−encoder was proposed for the classification of images and location detection of PQ disturbances. In [23], a CNN−GRU based network was proposed for the classification of seven PQ disturbances, achieving an accuracy of 98%. The input to the proposed network is a two−dimensional (2D) scalogram generated using short−time Fourier transform (STFT). Furthermore, this study provides the number of parameters for the most popular DL architectures. This information highlights why these models cannot be used without modifications for real−time application. In [24] a modified visual geometry group (VGG) architecture was proposed to classify and measure the duration of PQ disturbances. This study compared the performance of the model to that of DarkNet, AlexNet, ResNet, and VGG-16, demonstrating that the modified VGG outperforms these models. PQ disturbances are typically transformed into 2D signals and analyzed using deep neural networks for feature extraction and classification. In our study, we focus on preserving the 1D nature of the signal and utilizing a model capable of accurately classifying disturbances. This approach ensures that the system maintains the original signal structure, which is critical for the efficient implementation of hardware designed to operate in real−time. In [25], a comprehensive review of the DL algorithms used in PQ was presented. The authors highlighted several gaps in the field, such as models being treated as black boxes, scarcity of real datasets, and challenges in data labeling. This challenge is addressed by implementing a multi−label (ML) classification designed to identify and analyze multiple co-occurring disturbances simultaneously. This approach enhanced the detection process by enabling the algorithm to capture overlapping patterns, thereby improving the overall robustness and accuracy of the classification system. Furthermore, multi−class (MC) classification is explored and compared with the ML approach. This will ensure a deeper understanding of PQ issues, which will definitely help in devising more effective mitigation strategies and hence improving system reliability. In this study, we proposed a CNN−based model for detecting and classifying complex PQ disturbances. This problem was approached as a MC and ML classification challenge. The key contribution of this study are as follows:

1) Proposal of a framework based on CNNs for relevant feature extraction, that successfully characterizes PQ disturbances. This framework effectively captures the essential features of disturbances, thereby enabling a more accurate detection and classification.
2) Framework suitable for both MC and ML classification. This framework ensures robust and relevant feature extraction, making it adaptable to different classification tasks for the detection and classification of PQ disturbances. High accuracy in the classification of complex disturbances using both approaches.
3) The ML classification approach was the most effective method for detecting and classifying PQ disturbances. Through our experiments, we proved that ML classification outperformed the MC classification, particularly in distinguishing specific disturbances, by focusing on individual disturbances rather than their combinations.

The remainder of this paper is organized as follows. The second section explains the building blocks of the proposed architecture for feature extraction and classification, addressing MC and ML approaches. In the third section, we describe both approaches in detail, focusing on highlighting the differences in their classifications strategies.

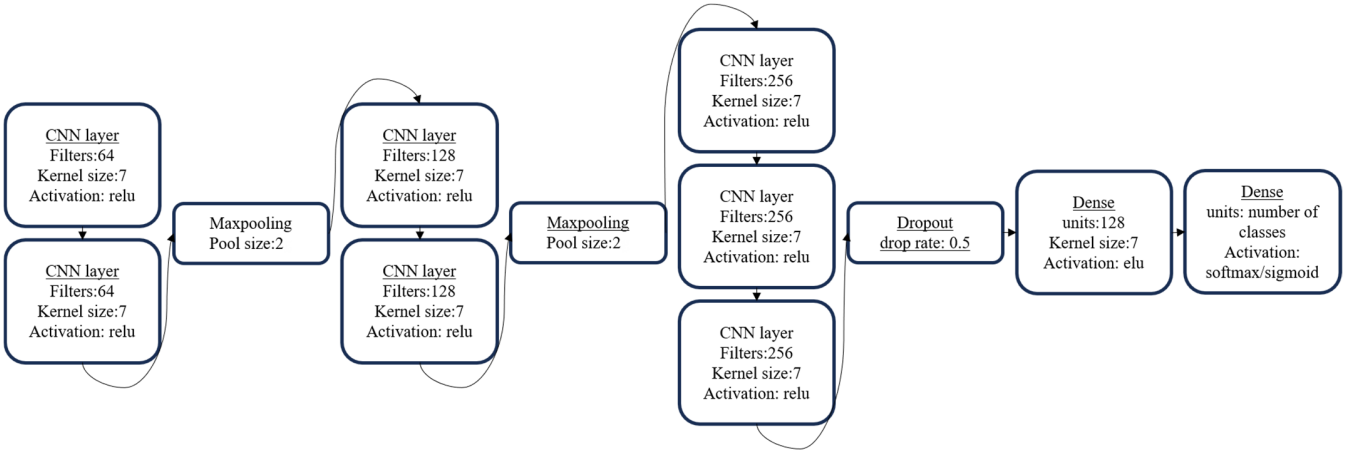

FIGURE 1. Architecture of proposed model.

Appropriate evaluation metrics are introduced in this section. The subsequent section presents the results obtained for various scenarios, along with a comprehensive comparison of the performance of each approach. Finally, the findings of the study are summarized, and conclusions are drawn in the final section.

II. DCNN ARCHITECTURE

Feature extraction plays a crucial role in the accuracy of PQ disturbance detection and classification. DL techniques simplify this process by enabling automated feature extraction, seamlessly combining it with classification, and by providing strong noise resistance. These qualities render DL particularly suitable for PQ applications [26]. Inspired by computer vision architectures, CNN are the most commonly used neural networks for this task. Typically, using WT and ST, disturbances are transformed into 2D data allowing models such as VGG, Inception, and CNN to handle feature extraction and classification [27]. In this study, we propose a deep CNN (DCNN) architecture inspired by VGG, which demonstrates that increasing network depth can positively impact classification accuracy and enhance performance across a variety of tasks and datasets [28]. Furthermore, the proposed architecture is designed to be implementable on hardware, enabling real−time operation for practical applications. The VGG-16 contains 16 layers with small 3×3 filters. In the proposed architecture, the number of layers was reduced to nine, and the kernel size was set to be 7×1. The architecture is illustrated in Fig. 1. The input to the DCNN was a 1D signal with a length of 1280. The signal was passed through several CNN layers, where the kernel size for all layers was set to 7×1, and the number of filters was 64, 128 and 256 for the first, second, and third blocks of the stacked CNN layers, respectively. In the CNN operations, the input undergoes convolution with a 7×1filter. The convolution was calculated using the following equation:

$$x\,[n] * g\,[n] = \sum_{m=-\infty}^{\infty} x\,[m]\, g[n-m] \tag{1}$$

where $x\,[n]$ is the input signal, $g\,[n]$ is the filter with which is made convolution and m denotes shifting. Initially, when the first seven points of $x\,[m]$ are multiplied by $g\,[-m]$ and summed, the filter is shifted to the right for n position and then with the appropriate points the convolution is calculated. The stride was set to be 1 and there was no zero padding. The weights of these filters are updated during training through backpropagation, which combines the feature extraction and classification. Weight updates are based on the gradient of the loss function, which is calculated in a way that minimizes this function. The output of each CNN layer was passed through an activation function. In our architecture, we primarily used a rectified linear unit (ReLU), which is known for its simplicity and efficiency. This was computed as follows:

$$f(x) = max(0, x) \tag{2}$$

The first two blocks are followed by a max−pooling layer with a pool size of 2. Pooling involves downsampling and helps prevent overfitting while reducing the complexity of the model. Max-pooling returns the maximum value within each window. For a 1D vector, the output vector $f_p\,(i)$ is calculated using the following equation:

$$f_p\,(i) = \max_{x \in R(i)} f(x) \tag{3}$$

where $R(i)$ is the pooling window of the input signal corresponding to the i-th output value.After the third CNN block, dropout was applied with a drop rate of 0.5, which is a regularization technique used to avoid overfitting by randomly excluding some neurons during training. The classification was performed using FC layers. In the FC layer, each neuron is connected to all neurons in the preceding layer and the first FC combines all the extracted features from the previous layers. An exponential linear unit (ELU) is used as an activation function that allows negative values. The ELU is defined using the following equation:

$$f\,(x) = \begin{cases} x, x > 0 \\ \alpha\,(\exp\,(x) - 1)\,, x \leq 0 \end{cases} \tag{4}$$

TABLE 1. Disturbances with corresponding labels and mathematical models.

Voltage Disturbances	Label	Mathematical model of PQ disturbances
Pure	C0	$x(t) = A\sin(\omega t - \varphi)$
Sag	C1	$x(t) = A\,(1 - \alpha(\mathrm{u}(t - t_1) - \mathrm{u}(t - t_2)))\sin(\omega t - \varphi)$
Swell	C2	$x(t) = A\,(1 + \beta(u(t - t_1) - u(t - t_2)))\sin(\omega t - \varphi)$
Interruption	C3	$x(t) = A\,(1 - \rho(u(t - t_1) - u(t - t_2)))\sin(\omega t - \varphi)$
Transient/Impulsive/Spike	C4	$x(t) = A[\sin(\omega t - \varphi) - \psi(e^{-750(t-t_a)} - e^{-344(t-t_b)})((u(t - t_a) - u(t - t_b)))]$
Oscillatory transient	C5	$x(t) = A[\sin(\omega t - \varphi) + \beta e^{-(t-t_{I1})/\tau}\sin(\omega_n(t - t_I) - \vartheta)((u(t - t_{I1}) - u(t - t_I)))]$
Harmonics	C6	$x(t) = A[\sin(\omega t - \varphi) + \sum_{n=3}^{7}\alpha_n\sin(n\omega t - \vartheta_n)]$
Harmonics + Sag	C7	$x(t) = A\,(1 - \alpha(u(t - t_1) - u(t - t_2)))[\sin(\omega t - \varphi) + \sum_{n'=3}^{5}\alpha_{n'}\sin(n'\omega t - \vartheta_{n'})]$
Harmonics + Swell	C8	$x(t) = A\,(1 + \beta(u(t - t_1) - u(t - t_2)))[\sin(\omega t - \varphi) + \sum_{n'=3}^{5}\alpha_{n'}\sin(n'\omega t - \vartheta_{n'})]$
Flicker	C9	$x(t) = A[1 + \lambda\sin(\omega_f t)]\sin(\omega t - \varphi)$
Flicker + Sag	C10	$x(t) = A[1 + \lambda\sin(\omega_f t) - \alpha(u(t - t_1) - u(t - t_2))]\sin(\omega t - \varphi)]$
Flicker + Swell	C11	$x(t) = A[1 + \lambda\sin(\omega_f t) + \beta(u(t - t_1) - u(t - t_2))]\sin(\omega t - \varphi)]$
Sag + Oscillatory transient	C12	$x(t) = A[\sin(\omega t - \varphi)(1 - \alpha(u(t - t_1) - u(t - t_2))) + \beta e^{-\frac{t-t_{I'}}{\tau}}\sin(\omega_n(t - t_{I'}) - \vartheta)((u(t - t_{II'}) - u(t - t_{I'})))]$
Swell + Oscillatory transient	C13	$x(t) = A[\sin(\omega t - \varphi)(1 + \beta(u(t - t_1) - u(t - t_2))) + \beta e^{-\frac{t-t_{I'}}{\tau}}\sin(\omega_n(t - t_{I'}) - \vartheta)((u(t - t_{II'}) - u(t - t_{I'})))]$
Notch	C14	$x(t) = A[\sin(\omega t - \varphi) - sign(\sin(\omega t - \varphi)\sum_{n=0}^{N\cdot c-1}k(u(t - (t_c + s\cdot n)) - u(t - (t_d + s\cdot n)))]$
Harmonics + Sag + Flicker	C15	$x(t) = A(1 + \lambda(\sin(\omega_f t))[\sin(\omega t - \varphi) + \sum_{n'=3}^{5}\alpha_{n'}\sin(n'\omega t - \vartheta_{n'})\,(1 - \alpha(\mathrm{u}(t - t_1) - \mathrm{u}(t - t_2)))$
Harmonics + Swell + Flicker	C16	$x(t) = A(1 + \lambda(\sin(\omega_f t))[\sin(\omega t - \varphi) + \sum_{n'=3}^{5}\alpha_{n'}\sin(n'\omega t - \vartheta_{n'})\,(1 + \beta(\mathrm{u}(t - t_1) - \mathrm{u}(t - t_2)))$
Harmonics + Sag + Oscillatory transient	C17	$x(t) = A[(1 - \alpha(\mathrm{u}(t - t_1) - \mathrm{u}(t - t_2))\sum_{n''=1}^{5}\alpha_{n''}\sin(n''\omega t - \vartheta_{n''}) + \beta e^{-\frac{t-t_I}{\tau}}\sin(\omega_n(t - t_I)\vartheta)((u(t - t_{II}) - u(t - t_I)))]$
Harmonics + Swell + Oscillatory transient	C18	$x(t) = A[(1 + \beta(\mathrm{u}(t - t_1) - \mathrm{u}(t - t_2))\sum_{n''=1}^{5}\alpha_{n''}\sin(n''\omega t - \vartheta_{n''}) + \beta e^{-\frac{t-t_I}{\tau}}\sin(\omega_n(t - t_I)\vartheta)((u(t - t_{II}) - u(t - t_I)))]$
Harmonics + Sag + Flicker+ Oscillatory transient	C19	$x(t) = A[(1 - \alpha(\mathrm{u}(t - t_1) - \mathrm{u}(t - t_2)))\sum_{n''=1}^{5}\alpha_{n''}\sin(n''\omega t - \vartheta_{n''}) + \beta e^{-\frac{t-t_I}{\tau}}\sin(\omega_n(t - t_I)\vartheta)((u(t - t_{II}) - u(t - t_I)))](1 + \lambda\sin(\omega_f t))$
Harmonics + Swell + Flicker+ Oscillatory transient	C20	$x(t) = A[(1 + \beta(\mathrm{u}(t - t_1) - \mathrm{u}(t - t_2))\sum_{n''=1}^{5}\alpha_{n''}\sin(n''\omega t - \vartheta_{n''}) + \beta e^{-\frac{t-t_I}{\tau}}\sin(\omega_n(t - t_I)\vartheta)((u(t - t_{II}) - u(t - t_I)))](1 + \lambda\sin(\omega_f t))$

Parameters used to define PQ disturbances: N=10, f=50 Hz

Sag/Swell/Interruption	Transients	Flicker	Oscillatory transient
N=10, f=50 Hz, $T \le t_2 - t_1 \le (N-1)T$ $0.1 \le \alpha \le 0.9$ $0.1 \le \beta \le 0.8$ $0.9 \le \rho \le 1.0$	$0.222 \le \psi \le 1.11$ $T \le t_a \le (N-1)T$ $t_b = t_a + 1ms$	$0.05 \le \lambda \le 0.1$ $8 \le f_f \le 25Hz$ $\omega_f = 2\pi f_f$	$300 \le f_n \le 900\ Hz;\ \omega_n = 2\pi f_n;\ 8ms \le \tau \le 40ms;\ -\pi \le \vartheta \le \pi$ $0.5T \le t_{II} - t_I \le \frac{N}{3.33}T$ $\frac{T}{5} \le t_{II'} - t_{I'} \le t_2 - t_1;\ t_{I'} \ge t_1;\ t_{II'} \le t_2$

Harmonics	Notch
$n = \{3,5,7\};\ 0.05 \le \alpha_n \le 0.15;\ -\pi \le \vartheta_n, \vartheta_{n'}, \vartheta_{n''} \le \pi$ $n' = \{3,5\};\ 0.05 \le \alpha_{n'} \le 0.15;$ $n'' = \{1,3,5\};\ \alpha_n \le 1 \wedge n'' = 1;\ 0.05 \le \alpha_{n''} \le 0.15 \wedge n'' = \{3,5\}$	$0.01T \le t_d - t_c \le 0.05T;\ t_d \le s;\ t_c \ge 0;\ 0.1 \le k \le 0.4;$ $c = \{1,2,4,6\};\ s = \frac{T}{c}$

where α is a parameter that controls the value for negative inputs. The last FC differs between the two approaches in terms of the number of neurons and activation function.

The output layer is a 1D vector, where each element represents the probability that the input belongs to a particular class or label. The length of this vector depends on whether the approach is for MC or ML classification. In Fig. 2, the block diagram of the proposed system is illustrated emphasizing the input and output components of the model.

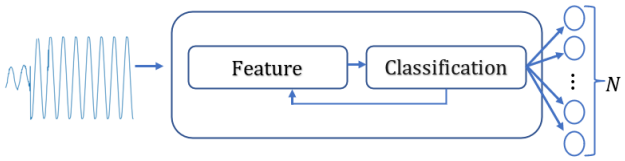

FIGURE 2. Block diagram of proposed framework for detection and classification of PQ disturbances.

III. MULTI– CLASS AND MULTI–LABEL CLASSIFICATION: STRATEGIES AND EVALUATION METRICS

The detection and classification of PQ disturbances using DL techniques shows great potential. In [25], a review of the latest DL applications and gaps in PQ disturbance classification was presented. This review highlights several challenges, including lack of novelty, insufficiently explained methods and experiments, reliance on synthetic data, and improper labeling of classes. Although labeling is straightforward with synthetically generated data, it often does not align with real−world scenarios, where labeling should be identical. This discrepancy creates issues because real PQ measurements are limited, thereby restricting the ability to accurately combine and analyze disturbances. Disturbances, such as sags, swells, harmonics, flicker, and oscillatory transients can interact and occur simultaneously, resulting in more complex waveform that are difficult to classify, thereby making the entire process more challenging. The mathematical models of the individual and complex disturbances used in our work, are presented in Table 1, and their waveforms are shown in Fig. 3. It is important that the features extracted from these images are distinguishable between the classes. To visualize the extracted features from the FC layer, we used the T-distributed Stochastic Neighbor Embedding (t-SNE) tool, which reduces the dimensionality of high−dimensional data [29]. The visual representation of the extracted features for the nine individual PQ disturbances, presented in TABLE 1, is shown in Fig. 4. Notably, they are well−separated with no overlap, indicating that the proposed model effectively extracts features specific to each class, thereby facilitating the classification process. At visual representation of the extracted features for the complex disturbances is shown in Fig. 5. Unlike Fig. 4, Fig.5 displays some overlap between classes. Overlapping occurs between classes that share common individual disturbances. This observation raises the question of whether the MC approach is an appropriate option for labeling and classifying PQ disturbances. There is ongoing discussion in the literature regarding the most appropriate approach for classifying samples that belong to multiple disturbance categories simultaneously. Most studies considered a combination of disturbances as an MC problem. However, this issue can also be addressed by ML classification, where multiple disturbances are assigned to a single instance. To the best of our knowledge, only a few studies have applied ML classification to the PQ field [30], [31], [32], [33]. Some frameworks [32], have also considered label correlation, which is important when dealing with a combination of disturbances. In our research we address the problem of both MC and ML classifications. The feature extraction component of the DCNN remains the same for both approaches, with the classification layer adapted specifically for either MC or ML classification.

A. MULTICLASS CLASSIFICATION

MC classification transforms the ML problem, such that each unique set of labels is treated as a separate class. The output is represented by a binary vector where each element corresponds to a class, and only one element is set to '1' to indicate the true class, while others are set to '0'. This approach is suitable when the label sets are determined based on real−world cases, and its advantage lies in capturing the relationships between the labels. However, a key drawback of MC is that it cannot handle unseen label combinations because it only considers label sets observed during training.

The analysis includes 21 scenarios of both isolated and combined disturbances, as reported in previous studies [7] and [34]. A FC layer with 21 neurons was used to classify 21 classes. Softmax is used to calculate the probability that an instance belongs to each class, where the sum of all the probabilities across classes is equal to one. The softmax function is calculated as follows:

$$Softmax(z_i) = \frac{e^{z_i}}{\sum_{j=1}^{C} e^{z_j}} \tag{5}$$

where z_i represents the raw score of the neuron in the final output before the activation function is applied. When $z_i$is passed through the softmax function, it becomes a probability. For the MC classification experiment, the model output was a 1D vector of length 21, where each element represented the probability of the input belonging to a particular class. In this approach, the input can belong to only one class, with the highest probability.

Categorical cross−entropy (CCE) is employed as a loss function in this architecture. It measures the difference between the true class label y_i and predicted probability distribution $\hat{y}_i$ across all classes. The CCE was calculated using the following equation:

$$CCE = -\sum_{i=1}^{N} y_i \log \hat{y}_i \tag{6}$$

1) EVALUATION METRICS

In MC classification, the most commonly used evaluation metrics are the accuracy, precision, recall, and F_1 score. They are calculated using the counts of true positives (TP), false positives (FP) and false negatives (FN). Accuracy measures the ratio of all correctly predicted samples to the total number of samples.

$$Accuracy = \frac{TP}{ALL} \tag{7}$$

Precision calculates the ratio of correctly predicted instances for a given class to all instances predicted to belong

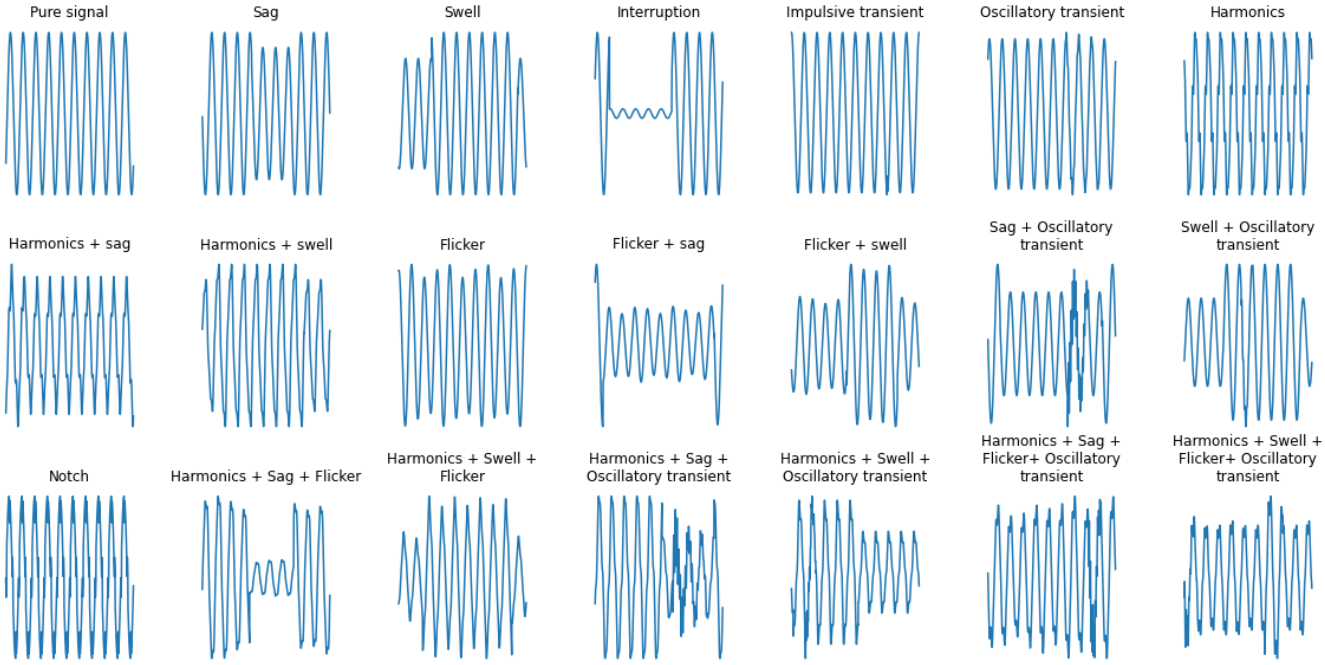

FIGURE 3. Waveforms of individual and complex PQ disturbances.

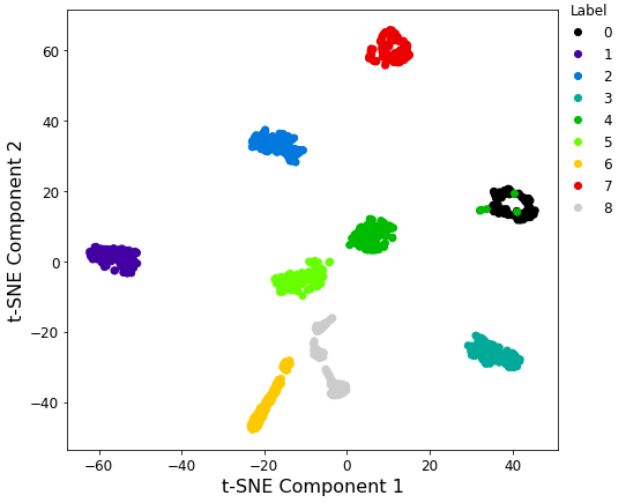

FIGURE 4. Visual representation of extracted features of individual PQ dis-turbances.

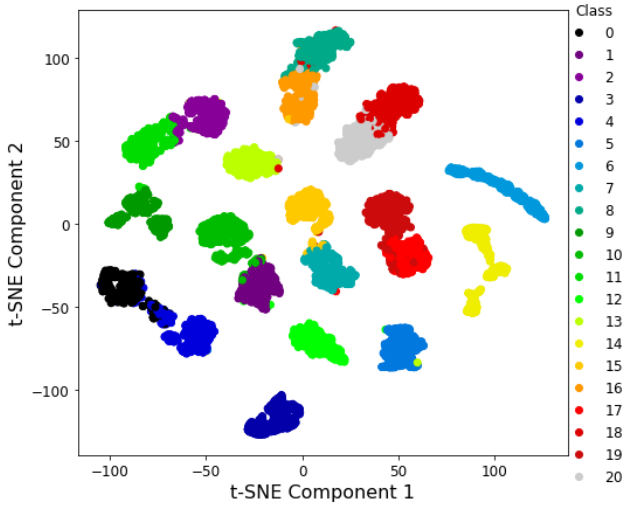

FIGURE 5. Visual representation of extracted features of individual complex disturbances.

to that class.

$$Precision = \frac{TP}{TP + FP} \tag{8}$$

Recall calculates the ratio of correctly predictions out of all actual positive instances.

$$Recall = \frac{TP}{TP + FN} \tag{9}$$

$F_1 - score$ calculates the harmonic mean between recall and precision.

$$F_1 - score = 2\frac{Precision \cdot Recall}{Precision + Recall} \tag{10}$$

B. MULTI-LABEL CLASSIFICATION

When the problem is treated as a ML classification task, we consider nine labels: pure, sag, swell, interruption, impulsive transient, oscillatory transient, harmonics, flicker, and notch. The target variables were represented by a binary vector, where the length corresponded to the total number of labels. Unlike the MC classification, where one−hot encoding is used, multi−hot encoding is applied here. This allows multiple '1' in the binary vector, indicating the presence of multiple labels. This approach enables the representation of all possible combinations of the nine labels, addressing

a gap in the literature related to real measurements of PQ disturbances, including how frequently they occur, and which combinations are most common.

A FC layer was employed to classify the labels. The sigmoid function $\sigma(x)$, was used as the activation function which calculated the probability for each disturbance independently, producing values between 0 and 1. The sigmoid function is represented as:

$$\sigma(z) = \frac{1}{1 + e^{-z}} \tag{11}$$

In summary, for the ML classification experiment, the model output is a 1D vector of length nine, where each element represents the probability of the presence of the corresponding label. The output layer used a sigmoid activation function that independently which produced probabilities for each label.

Binary cross−entropy (BCE) is a loss function used to calculate the error between real and predicted values in the binary classification problem. In ML classification, BCE is applied across all labels, summing the loss for each label and focusing on minimizing this total loss during training. BCE loss was calculated using the following equation:

$$BCE = -\frac{1}{N}\sum_{i=1}^{N}\left[y_i \log(\hat{y}_i) + (1 + y_i)\log(1 - \hat{y}_i)\right] \tag{12}$$

where,

- N is the number of instances
- y_i is the set of true values for the i-th instance
- $\hat{y}_i$ is predicted probability for the i-th instance

This equation calculates the loss for each label and sums the total loss across the labels to guide model optimization.

1) EVALUATION METRICS

In ML classification, where the target vector is represented using multi−hot encoding, the evaluation metrics differ from those used in the MC classification. Based on [30] and [35], several evaluation metrics were used in this study. One of the key metrics is the Hamming loss (HL), which calculates the difference between predicted and real values by measuring the fraction of misclassified labels. This is one of the most commonly used metrics for ML classification. HL was calculated using the following equation:

$$HL = \frac{1}{N \cdot L}\sum_{i=1}^{N}\sum_{j=0}^{L} 1(y_{ij} \neq \hat{y}_{ij}) \tag{13}$$

where

- L is the total number of labels
- $1(y_{ij} = \hat{y}_{ij})$ is an indicator function that has a value of 1 when the predicted labels $\hat{y}$ differ from the true labels y_i

To provide a clearer understanding of the performance of the proposed model, the HL for each label was calculated using (13).

$$HL_j = \frac{1}{N}\sum_{i=1}^{N} 1(y_{ij} \neq \hat{y}_{ij}) \tag{14}$$

Subset accuracy or exact match ratio measures the proportion of samples in which all labels are predicted exactly as the true set of labels.

$$Subset\ Accuracy = \frac{1}{N}\sum_{i=1}^{N} 1(y_i = \hat{y}_i) \tag{15}$$

This metric is useful when an exact set of labels is important for the problem. One drawback of this metric is that it is sensitive to class imbalances.

However, it is important to calculate the accuracy of each label. That can be calculated using the following equation:

$$Acc_j = \frac{1}{N}\sum\nolimits_{i=1}^{N} 1(y_{ij} = \hat{y}_{ij}) \tag{16}$$

Ranking loss (RL) calculates the average error of the label order.

$$RL = \frac{1}{N}\sum\nolimits_{i=1}^{N} \frac{1}{\left|y_i^+\right|\left|Y_i^-\right|}\sum\nolimits_{y^+ \in Y_i^+}\sum\nolimits_{y^- \in Y_i^+} 1\left(\hat{y}_i^+ \leq \hat{y}_i^-\right) \tag{17}$$

One error (OE) refers to the probability that a top−ranked label is incorrect.

$$OE = \frac{1}{N}\sum\nolimits_{i=1}^{N} 1\left(\arg\max_{y \in L} \hat{y}_i \notin y_i^+\right) \tag{18}$$

where

- y_i^+ is the set of relevant labels for the i$^{\text{th}}$ instance
- y_i^- is the set of irrelevant labels for the i$^{\text{th}}$ instance
- $\hat{y}_i$ is the predicted score for i$^{\text{th}}$ instance
- $1\left(\hat{y}_i^+ \leq \hat{y}_i^-\right)$ is an indicator function that equals one if the score of the relevant labels is lower than or equal to the score of irrelevant labels.

The micro−evaluation metrics calculate the precision, recall, and F_1 score using the total counts of TP, FP, and FN. Micro metrics are suitable when data are unbalanced.

$$Precison_{micro} = \frac{\sum TP}{\sum TP + FP} \tag{19}$$

$$Recall_{micro} = \frac{\sum TP}{\sum TP + FN} \tag{20}$$

$$F_1 - score_{micro} = 2\frac{Precison_{micro} \cdot Recall_{micro}}{Precison_{micro} + Recall_{micro}} \tag{21}$$

IV. RESULTS

A synthetically generated dataset is used to train and evaluate the performance of the model. The dataset contains 42000 synthetically generated signals created using the mathematical models described in [36]. These signals were further modified by adding Gaussian noise and applying phase shift. Out of the total signals, 18000 contain a single disturbance, 12000 signals contain combination of two disturbance, 8000 have three disturbances and 4000 contain four disturbances.

In this study, a DCNN is proposed for the classification of PQ disturbances. All signals had a frequency of 50 Hz and were sampled at $f_s = 6400$Hz, they were 10 periods long. The dataset is divided into three subsets: training (70%),

validation(10%) and testing (20%). The models were validated in both noiseless and noisy environments, where the signal−to−noise ratio (SNR) were 20 dB, 30 dB, 40 dB, and 50 dB, as well as in a mixed SNR scenario. Two different approaches are considered for labeling PQ deviation, MC and ML classification. The learning curves for the training and validation datasets are shown in Fig.6. It is evident from these curves that the accuracy of the model converges with no indication of overfitting. The training speed depends on the learning rate. If the learning rate is high, the training is fast, however, the accuracy and loss fluctuate, and the model may not converge. Conversely, with a low learning rate, the training process is slow, and the function tends to converge, however, the model risks overfitting. The learning rate was set to 0.0003 and the Adam optimizer was used. As shown in Fig. 6, the learning curves for the DCNN model during the training and validation sets indicate that the chosen learning rate was appropriate. There were no fluctuations, and the curves converged rapidly. Moreover, the validation curve closely followed the training curve with no signs of overfitting. An early stopping technique was applied to halt the training process when no improvement in the loss function was observed for five epochs.

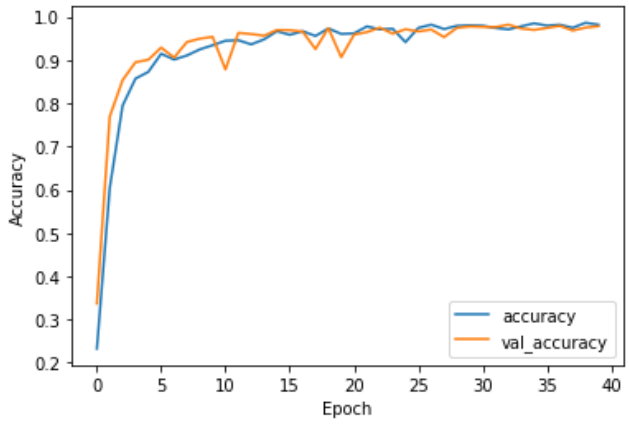

FIGURE 6. Accuracy curve for training and validation dataset through training.

In TABLE 2, the archived accuracy for different levels of noise is presented. When the SNR was 20 dB, the accuracy reached is 91.4 %, with misclassifications primary occurring for pure sine and impulsive transients, as expected. When the data consist of a mix of noiseless signals and signals with added noise, where the SNR ranges from 30−50 dB, the achieved accuracy increases to 98.03%. Additionally, TABLE 2 includes results from classification models integrated into the block architecture proposed in [31], allowing for a comparison of performance across different model configurations. In TABLE 3, three additional evaluation metrics: precision, recall and F_1 score are provided to offer a detailed view of the model's performance. These metrics were calculated for the mixed dataset. These results indicate that the model performed exceptionally well. However,

TABLE 2. MC classification accuracy [%].

	Without noise	50 dB	40 dB	30 dB	20 dB	Mix data
DCNN (proposed)	98.64	98.7	98.5	97.6	91.4	98.03
INCEPTION-GRU	93	92.3	91.9	89.6	82.8	88.1
ResNet - GRU	97.3	97.1	96.9	92.17	83	96.08
RESnet18	98.4	98.2	97.9	96.4	92.9	97.7

TABLE 3. Model performance across classes.

Class	Precision	Recall	F_1 score
C0	0.90	0.97	0.93
C1	0.99	0.99	0.99
C2	0.99	1.00	1.00
C3	1.00	1.00	1.00
C4	0.96	0.92	0.94
C5	1.00	0.99	0.99
C6	1.00	1.00	1.00
C7	0.95	1.00	0.98
C8	0.99	0.99	0.99
C9	0.99	1.00	0.99
C10	1.00	0.98	0.99
C11	1.00	0.99	0.99
C12	1.00	0.99	0.99
C13	0.99	1.00	0.99
C14	1.00	1.00	1.00
C15	0.99	0.95	0.97
C16	0.99	0.99	0.99
C17	0.95	0.99	0.97
C18	0.98	0.98	0.98
C19	0.99	0.95	0.97
C20	0.98	0.98	0.98

misclassification primarily occurs between pure sine and impulsive transients owing to the high level of added noise. It is notable, 90% of signals classified as pure sine are indeed pure sine, with the remainder belonging to the impulsive transient class. Additionally, 97% of all pure sine signals were correctly classified, while 92% of signals with impulsive transient were accurately classified. The proposed model also demonstrated a high accuracy when classifying signals with a combination of multiple disturbances. This observation indicates that the model detects and classifies PQ disturbances, making it highly suitable for scenarios in which possible

TABLE 4. Accuracy and Hamming loss calculated for each label at different SNR level.

	20 dB		30 dB		40 dB		50 dB		Noiseless	
Label	HL	Acc.	HL	Acc.	HL	Acc.	HL	Acc.	HL.	Acc.
Pure	0.05	94.9	0.012	98.7	0.001	99.8	0.0007	99.9	0.0002	99.9
Sag	0.004	99.5	0.0004	99.9	0.001	99.8	0.0007	99.9	0.001	99.8
Swell	0.002	99.7	0.0013	98.6	0.001	99.8	0.002	99.7	0.002	99.7
Interruption	0.0005	99.9	0	100	0	100	0	100	0	100
Transient	0.05	95	0.0141	98.5	0.001	99.8	0.0004	99.9	0.0002	99.9
Oscillatory transient	0.011	98.8	0.001	99.8	0.0008	99.9	0.0003	99.9	0.0004	99.9
Harmonics	0.0003	99.9	0	1	0.0001	99.9	0.0001	99.8	0	100
Flicker	0.012	98.7	0.002	99.7	0.002	99.7	0.001	99.8	0.002	99.7
Notch	0.02	97.2	0.01	98.7	0.0128	98.7	0.011	98.8	0.01	98.8

combinations of disturbances are well understood. The results achieved when classification is treated as ML problem are presented in TABLE 4, TABLE 5, and TABLE 6, respectively. In TABLE 4, the accuracy and HL for each label in ML classification were calculated independently for different SNR. The presented results indicate that the accuracy is predominantly above 98%, except for pure and transient disturbances in high−noise environments. These results highlight the remarkable performance of the proposed model on each label.

In TABLE 5, the values for accuracy, HL, RL, and OE for the models used in the ML classification are presented. The ResNet18 model was not included in the table because its performance was unacceptable, with an accuracy below 50%. From the results, it is evident that the proposed model exhibits an excellent performance in ML classification. The model achieved 98.5% accuracy in predicting the correct label set for mixed dataset. Although ResNET performs better than Inception−GRU, its performance decreases in noisy environments, therby highlighting the robustness and superior performance of the proposed architecture. In TABLE 6, the results for micro precision, micro recall and micro F_1 scores are presented for the mixed dataset. Because the dataset was imbalanced, with the number of instances for sag and swells being dominant, the evaluation metrics were chosen to accurately reflect the overall performance. The micro−metrics confirm the outstanding performance of the proposed model, especially in handling imbalanced data.

The receiver operating characteristic (ROC) curve is typically used in binary classifiers, but it can also be applied to ML classification. The ROC curve illustrates the trade−off between the true positive rate (recall) and false positive rate (FTP). The quality of the classifier is represented by the area under the curve (AUC), with the best possible ROC curve having an AUC close to 1. The ROC curves for each class are shown in Fig. 7. The model demonstrated excellent performance, with the AUC for each class being close to 1. Specifically, for the impulsive transient, the AUC was 0.99. Considering all the evaluation metrics discussed, it is clear that the proposed DCNN model performs well in ML classification of PQ disturbances.

TABLE 5. Performance of different model.

	No noise	50 dB	40 dB	30 dB	20 dB	Mix data
			Accuracy			
DCNN	99	99.01	98.76	97.25	91.7	98.56
INCEPTION -GRU	59.7	62.3	63.2	57.5	53	61.4
ResNet - GRU	89	88.8	89.4	86.7	67.7	87.8
			Hamming Loss			
DCNN	0.001	0.001	0.002	0.004	0.019	0.002
INCEPTION -GRU	0.047	0.045	0.44	0.051	0.056	0.047
ResNet - GRU	0.016	0.016	0.016	0.018	0.049	0.018
			Ranking Loss			
DCNN	0.0001	0.0001	0.0001	0.001	0.007	0.0002
INCEPTION -GRU	0.168	0.16	0.15	0.2	0.21	0.173
ResNet - GRU	0.006	0.007	0.006	0.007	0.02	0.007
			One-error			
DCNN	0.0004	0.0004	0.0003	0.01	0.05	0.002
INCEPTION -GRU	0.05	0.06	0.06	0.1	0.09	0.07
ResNet - GRU	0.04	0.05	0.05	0.018	0.1	0.05

TABLE 6. Performance of proposed architecture.

	Micro precision	Micro Recall	Micro F_1 score
Mix data	99.6	99.3	99.4

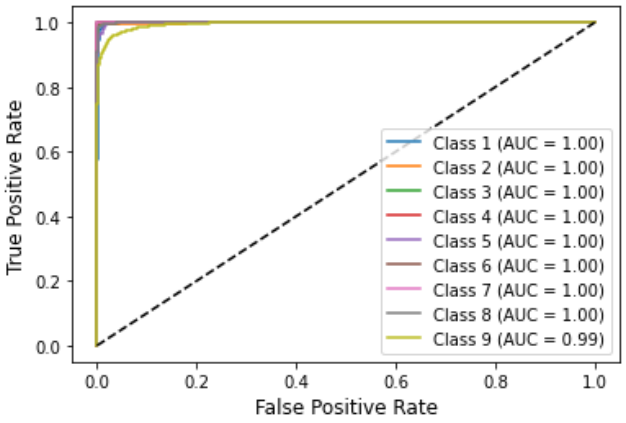

FIGURE 7. ROC curve for each class.

TABLE 7. Training model performance.

Parameters	MC	ML
Number of model parameters	10953045	10951497
Training time	116 min	116.1 min
Elapsed epochs	39	39
Best validation loss	0.054	0.004

The training model parameters are listed in TABLE 7. The total number of parameters is approximately 10 million. For comparison, VGG-16 has approximately 138 million parameters, ResNet-50 has around 20 million parameters, while ResNet-100 has approximately 40 million parameters. The training time for the proposed model was 116.1 minutes on a central processing unit.

V. CONCLUSION

In this study, a DCNN architecture was proposed for the classification of complex PQ disturbances. The features extracted by this architecture are highly discriminative, significantly enhancing the classification performance.

These features are suitable for both MC and ML classification approaches. The results demonstrated excellent accuracy in both MC and ML classifications across various conditions.

The model was evaluated on phase−shifted signals with an SNR ranging from 20 dB to 50 dB, proving its robustness in noisy environments. An important conclusion from the results is that the ML classification approach outperforms the MC approach for classifying complex PQ disturbances.

Furthermore, the performance of the model surpassed that of other state−of−the−art models for PQ disturbance classification. Future work will focus on reducing computational costs and implementing the model on hardware suitable for real−time applications.

ACKNOWLEDGMENT

Views and opinions expressed are however those of the author(s) only and do not necessarily reflect those of the European Union. Neither the European Union nor the granting authority can be held responsible for them.

REFERENCES

[1] *IEEE Recommended Practice for Monitoring Electric Power Quality*, Standard IEEE Std. 1159-2009, 2009, doi: 10.1109/IEEESTD.2009.5154067.

[2] *Electromagnetic Compatibility (EMC)-Part 4-7: Testing and Measurement Techniques-General Guide on Harmonics and Interharmonics Measurement and Instrumentation, for Power Supply Systems and Equipment Connected Thereto*, Standard IEEE Std. IEC 61000-4-7:2002, 2008.

[3] P. Gonzalez, E. Romero-Cadaval, E. Gonzalez, and M. A. Guerrero, "Impact of grid connected photovoltaic system in the power quality of a distribution network," in *Proc. Doctoral Conf. Comput., Elect. Ind. Syst.*, Berlin, Germany, L. M. Camarinha-Matos, Ed., Cham, Switzerland: Springer, Feb. 2011, pp. 466–473, doi: 10.1007/978-3-642-19170-1_51.

[4] S. H. Aleem, A. Y. Abdelaziz, and A. F. Zobaa, "Egyptian grid code of wind farms and power quality," in *Handbook of Distributed Generation*. Cham, Switzerland: Springer, 2017, doi: 10.1007/978-3-319-51343-0.

[5] W. Liu, H. Xu, S. Niu, and J. Xie, "Optimal distributed generator allocation method considering voltage control cost," *Sustainability*, vol. 8, no. 2, p. 193, Feb. 2016, doi: 10.3390/su8020193.

[6] J. Milanovic, "CIGRE/CIRED JWG C4. 112: Guidelines for power quality monitoring-measurement locations, processing and presentation of data," *Electra*, vol. 227, pp. 42–47, 2014.

[7] M. Markovska, D. Taskovski, Z. Kokolanski, V. Dimchev, and B. Velkovski, "Real-time implementation of optimized power quality events classifier," *IEEE Trans. Ind. Appl.*, vol. 56, no. 4, pp. 3431–3442, Jul. 2020, doi: 10.1109/TIA.2020.2991950.

[8] A. Yılmaz, A. Küçüker, G. Bayrak, D. Ertekin, M. Shafie-Khah, and J. M. Guerrero, "An improved automated PQD classification method for distributed generators with hybrid SVM-based approach using undecimated wavelet transform," *Int. J. Electr. Power Energy Syst.*, vol. 136, Mar. 2022, Art. no. 107763, doi: 10.1016/j.ijepes.2021.107763.

[9] S. Jamali, A. R. Farsa, and N. Ghaffarzadeh, "Identification of optimal features for fast and accurate classification of power quality disturbances," *Measurement*, vol. 116, pp. 565–574, Feb. 2018.

[10] H. Erişti, Ö. Yıldırım, B. Erişti, and Y. Demir, "Optimal feature selection for classification of the power quality events using wavelet transform and least squares support vector machines," *Int. J. Electr. Power Energy Syst.*, vol. 49, pp. 95–103, Jul. 2013, doi: 10.1016/j.ijepes.2012.12.018.

[11] D. De Yong, S. Bhowmik, and F. Magnago, "An effective power quality classifier using wavelet transform and support vector machines," *Expert Syst. Appl.*, vol. 42, nos. 15–16, pp. 6075–6081, Sep. 2015, doi: 10.1016/j.eswa.2015.04.002.

[12] R. Kumar, B. Singh, D. T. Shahani, A. Chandra, and K. Al-Haddad, "Recognition of power-quality disturbances using S-transform-based ANN classifier and rule-based decision tree," *IEEE Trans. Ind. Appl.*, vol. 51, no. 2, pp. 1249–1258, Mar. 2015, doi: 10.1109/TIA.2014.2356639.

[13] S. Banerjee and P. Sarathee Bhowmik, "Machine learning based classifiers for dynamic and transient disturbance classification in smart microgrid system," *Measurement*, vol. 240, Jan. 2025, Art. no. 115576, doi: 10.1016/j.measurement.2024.115576.

[14] S. Dash and U. Subudhi, "Multiple power quality event detection and classification using wavelet transform and random forest classifier," in *Proc. Int. Conf. Appl. Electromagn., Signal Process. Commun. (AESPC)*, vol. 1, Oct. 2018, pp. 1–5, doi: 10.1109/AESPC44649.2018.9033313.

[15] G. Singh, Y. Pal, and A. K. Dahiya, "Classification of power quality disturbances using linear discriminant analysis," *Appl. Soft Comput.*, vol. 138, May 2023, Art. no. 110181, doi: 10.1016/j.asoc.2023.110181.

[16] M. Liu, Y. Chen, Z. Zhang, and S. Deng, "Classification of power quality disturbance using segmented and modified S-transform and DCNN-MSVM hybrid model," *IEEE Access*, vol. 11, pp. 890–899, 2023, doi: 10.1109/ACCESS.2022.3233767.

[17] R. S. Salles and P. F. Ribeiro, "The use of deep learning and 2-D wavelet scalograms for power quality disturbances classification," *Electr. Power Syst. Res.*, vol. 214, Jan. 2023, Art. no. 108834, doi: 10.1016/j.epsr.2022.108834.
[18] S. Pan, X. Nie, X. Zhai, B. Wang, H. Ge, C. He, and Z. Ding, "Classification of power quality disturbances using resnet with channel attention mechanism," 2024, *arXiv:2407.04739*.
[19] S. Wang and H. Chen, "A novel deep learning method for the classification of power quality disturbances using deep convolutional neural network," *Appl. Energy*, vol. 235, pp. 1126–1140, Feb. 2019, doi: 10.1016/j.apenergy.2018.09.160.
[20] M. Wang, Z. Deng, Y. Zhang, and Z. Zhu, "An automatic identification framework for complex power quality disturbances based on ensemble CNN," *IEEE Access*, vol. 11, pp. 56550–56560, 2023, doi: 10.1109/ACCESS.2023.3273294.
[21] R. Gong and T. Ruan, "A new convolutional network structure for power quality disturbance identification and classification in micro-grids," *IEEE Access*, vol. 8, pp. 88801–88814, 2020, doi: 10.1109/ACCESS.2020.2993202.
[22] P. Khetarpal, N. Nagpal, M. S. Al-Numay, P. Siano, Y. Arya, and N. Kassarwani, "Power quality disturbances detection and classification based on deep convolution auto-encoder networks," *IEEE Access*, vol. 11, pp. 46026–46038, 2023, doi: 10.1109/ACCESS.2023.3274732.
[23] E. Yiğit, U. Özkaya, Š. Öztürk, D. Singh, and H. Gritli, "Automatic detection of power quality disturbance using convolutional neural network structure with gated recurrent unit," *Mobile Inf. Syst.*, vol. 2021, pp. 1–11, Jul. 2021, doi: 10.1155/2021/7917500.
[24] C. Iturrino-García, G. Patrizi, A. Bartolini, L. Ciani, L. Paolucci, A. Luchetta, and F. Grasso, "An innovative single shot power quality disturbance detector algorithm," *IEEE Trans. Instrum. Meas.*, vol. 71, pp. 1–10, 2022, doi: 10.1109/TIM.2022.3201927.
[25] R. A. D. Oliveira and M. H. J. Bollen, "Deep learning for power quality," *Electr. Power Syst. Res.*, vol. 214, Jan. 2023, Art. no. 108887, doi: 10.1016/j.epsr.2022.108887.
[26] S. U. Khan, M. Mynuddin, D. M. A. Ahad, M. I. Hossain, M. J. Islam, and M. F. Kabir, "A comparative analysis of deep learning models for power quality disturbance classification," in *Proc. IEEE World AI IoT Congr. (AIIoT)*, Seattle, WA, USA, Jun. 2023, pp. 0317–0323, doi: 10.1109/AIIOT58121.2023.10174320.
[27] K. Cai, W. Cao, L. Aarniovuori, H. Pang, Y. Lin, and G. Li, "Classification of power quality disturbances using wigner-ville distribution and deep convolutional neural networks," *IEEE Access*, vol. 7, pp. 119099–119109, 2019, doi: 10.1109/ACCESS.2019.2937193.
[28] K. Simonyan and A. Zisserman, "Very deep convolutional networks for large-scale image recognition," 2014, *arXiv:1409.1556*.
[29] L. J. P. van der Maaten and G. E. Hinton, "Visualizing high-dimensional data using t-SNE," *J. Mach. Learn. Res.*, vol. 9, pp. 2579–2605, Nov. 2008.
[30] Y. Luo, K. Li, Y. Li, D. Cai, C. Zhao, and Q. Meng, "Three-layer Bayesian network for classification of complex power quality disturbances," *IEEE Trans. Ind. Informat.*, vol. 14, no. 9, pp. 3997–4006, Sep. 2018, doi: 10.1109/TII.2017.2785321.
[31] X. Xiao and K. Li, "Multi-label classification for power quality disturbances by integrated deep learning," *IEEE Access*, vol. 9, pp. 152250–152260, 2021, doi: 10.1109/ACCESS.2021.3124511.
[32] Z. Wang, T. Deng, H. Wang, J. Tao, H. Zhang, and Q. Wang, "Power quality disturbance recognition method in park distribution network based on one-dimensional VGGNet and multi-label classification," in *Proc. 5th Asia Energy Electr. Eng. Symp. (AEEES)*, Chengdu, China, Mar. 2023, pp. 764–770, doi: 10.1109/AEEES56888.2023.10114115.
[33] Y. Dong, H. Cao, X. Ding, G. Xu, and C. Yue, "Multi-task learning method for classification of multiple power quality disturbances," *IET Gener., Transmiss. Distrib.*, vol. 14, no. 5, pp. 900–909, Mar. 2020.
[34] A. Zlatkova, M. Markovska, and D. Taskovski, "Deep learning approach for classification of PQ disturbances," in *Proc. IEEE Int. Conf. Environ. Electr. Eng. IEEE Ind. Commercial Power Syst. Eur. (EEEIC/I&CPS Eur.)*, Prague, Czech Republic, Jun. 2022, pp. 1–6, doi: 10.1109/EEEIC/ICPSEUROPE54979.2022.9854673.
[35] J. Bogatinovski, L. Todorovski, S. Džeroski, and D. Kocev, "Comprehensive comparative study of multi-label classification methods," *Expert Syst. Appl.*, vol. 203, Oct. 2022, Art. no. 117215, doi: 10.1016/j.eswa.2022.117215.
[36] R. Igual, C. Medrano, F. J. Arcega, and G. Mantescu, "Mathematical model of power quality disturbances," Mendeley Data, V1, doi: 10.17632/6kmkk9bjdx.1.

ALEKSANDRA ZLATKOVA (Member, IEEE) was born in Shtip, North Macedonia, in 1996. She received the B.E. and M.E. degrees in electrical engineering and information technologies from Ss. Cyril and Methodius University in Skopje, North Macedonia. She is currently pursuing the Ph.D. degree in electrical engineering and information technologies. Her research interests include signal processing, deep learning, and power quality.

DIMITAR TASKOVSKI (Senior Member, IEEE) received the Ph.D. degree in electrical engineering from Ss. Cyril and Methodius University in Skopje, North Macedonia, in 2004. He is currently a Full Professor with the Faculty of Electrical Engineering and Information Technologies, Ss. Cyril and Methodius University in Skopje. His research interests include wavelet theory and filter banks, data hiding and watermarking, machine learning, and power quality analysis.